Study of heat transfer in steady flows of Carreau fluids near a stretching cylinder using numerical solutions

by

Iram Showkat

Reg. No. 00000330981

A dissertation submitted in partial fulfillment of the requirements for the degree of Master of Philosophy in Mathematics

Supervised by

Prof. Meraj Mustafa Hashmi

Department of Mathematics, School of Natural Sciences, National University of Sciences and Technology, Islamabad, Pakistan

FORM TH-4

National University of Sciences & Technology

MS THESIS WORK

We hereby recommend that the dissertation prepared under our supervision by: **IRAM SHOWKAT**, Regn No. **00000330981** Titled: **"Study of Heat Transfer in Steady Flows of Carreau Fluids Near a Stretching Cylinder Using Numerical Solutions"** accepted in partial fulfillment of the requirements for the award of **MS** degree.

Examination Committee Members

1. Name: DR. MUHAMMAD ASIF FAROOQ Signature: _____

2. Name: DR. AHMAD JAVID Signature: _____

Supervisor's Name: DR. MERAJ MUSTAFA HASHMI Signature: _____

_____ 30/08/2022
Head of Department Date

COUNTERSINGED

Date: 31.8.2022 _____
Dean/Principal

This dissertation is dedicated to my loving parents and brother

for their endless love, prayers and support.

Acknowledgments

Praise be to Allah, the Almighty, for the blessings and mercies, the health, and the inspirations that he gave me to complete my MS.

I consider it an honor to express my heartfelt appreciation to my respected supervisor prof. Meraj Mustafa Hashmi for his continued support during my research, for his patience and motivation. During the study and writing time of this thesis, he kept me well-directed and focused.

I would like to express my sincere thanks to the members of my GEC, Dr. Muhammad Asif Farooq and Dr Ahmad Javed for their support and guidance in completing this thesis.

This recognition will be worthless unless I give my heartfelt veneration to my loving parents over the difficult time of this research for their sacrifices, tremendous efforts, excellent contributions, financial help and motivation.

Iram Showkat

Table of Contents

Acknowledgments i
Table of Contents ii
List of Figures iv
List of Tables vi
Abstract vii
Chapter 1 1
Introduction 1
1.1 Fundamental definitions 1
1.1.1 Compressible and incompressible flows 1
1.1.2 Steady and unsteady flows 1
1.1.3 Newtonian fluids 1
1.1.4 Non-Newtonian fluids 1
1.1.5 Shear-thinning fluids/Shear-thickening fluids 2
1.2 Mathematical models for shear-thinning/shear-thickening fluids 3
1.2.1 Power-law model 3
1.2.2 Cross fluid model 3
1.3 Boundary layer formation 3
1.4 Some Dimensionless Numbers 4
1.4.1 Reynolds number 4
1.4.2 Prandtl number 5
1.4.3 Nusselt number 5
1.4.4 Eckert number 5
1.5 Fluid flow over a stretching cylinder 5
1.6 Heat transfer 7
1.6.1 Conduction 7
1.6.2 Convection 8
1.6.3 Radiation 8
1.7 Literature review 8
Chapter 2 11
Novel numerical results for heat transfer along a stretching cylinder immersed in a shear-thinning fluid 11

2.1 Introduction 11
2.2 Problem formulation 11
2.3 Some particular cases 14
2.4 Method of solution 15
2.5 Numerical results and discussion 15
2.6 Concluding remarks 21
Chapter 3 23
3.1 Introduction 23
3.2 Basic equations and problem formulation 23
3.3 Particular cases 26
3.3.1 Flat surface case 26
3.3.2 Newtonian fluid case 26
3.4 Method of solution 26
3.5 Results and discussion 27
3.6 Concluding remarks 33
Bibliography 35

List of Figures

Fig. 1.1: Boundary layer flow 4

Fig 1.2 (a): Axial velocity curves at various values of $\boldsymbol{M}$ when $\boldsymbol{Pr = 5}$..... 7
Fig 1.2 (b): Dimensionless temperature $\boldsymbol{\theta(\eta)}$ for a variety of $\boldsymbol{M}$ values when $\boldsymbol{Pr = 5}$..... 7

Fig. 2.1: A schematic of fluid flow over a cylindrical surface 14

Fig. 2.2 (a): Distribution of axial velocity field for various choices of curvature parameter *M*... 18
Fig. 2.2 (b): Distribution of temperature field for various choices of curvature parameter *M*..... 18

Fig. 2.3 (a): Distribution of axial velocity field for various choices of magnetic interaction parameter *Ha*..... 18
Fig. 2.3 (b): Distribution of temperature field for various choices of magnetic interaction parameter *Ha*..... 18

Fig. 2.4 (a): Distribution of axial velocity field for various choices of flow index behavior *n*.... 19
Fig. 2.4 (b): Distribution of temperature field for various choices of flow index behavior *n* 19

Fig. 2.5 (a): Distribution of axial velocity field for various choices of local Weissenberg number *K*..... 19
Fig. 2.5 (b): Distribution of temperature field for various choices of local Weissenberg number *K* 19

Fig 2.6: Variation of temperature $\boldsymbol{\theta}$ with $\boldsymbol{\eta}$ by changing values of Eckert number..... 20

Fig. 2.7 (a): Variation in skin friction coefficient for the different values of curvature parameter *M* 20
Fig. 2.7 (b): Variation in Nussselt number for different values of curvatutre parameter $\boldsymbol{M}$..... 20

Fig. 3.1: Distribution of axial velocity field for varying choices of mixed convection parameter $\boldsymbol{\gamma}$. 30
Fig. 3.2: Distribution of temperature field for a variety of $\boldsymbol{Pr}$ values. 30
Fig. 3.3: Distribution of axial velocity field for various values of magnetic interaction parameter $\boldsymbol{Ha}$. 30
Fig. 3.4: Distribution of temperature field for various values of $\boldsymbol{Ha}$ values when $\boldsymbol{K = 0\ and\ K = 5}$. 30
Fig. 3.5: Distribution of axial velocity field for various choices of curvature parameter $\boldsymbol{M}$..... 31

Fig. 3.6: Distribution of temperature field for a variety of $\boldsymbol{M}$ values. 31
Fig. 3.7: Distribution of axial velocity field for various choices of flow behavior index $\boldsymbol{n}$..... 31
Fig. 3.8: Distribution of axial velocity field for various choices of local Wessienberg number $\boldsymbol{K}$. 31
Fig. 3.9: Variation in skin friction coefficient with $\boldsymbol{n}$ for several values of curvature parameter $\boldsymbol{M}$..... 32
Fig. 3.10: Variation in Nusselt number with $\boldsymbol{n}$ for several values of curvature parameter $\boldsymbol{M}$..... 32

List of Tables

Table 2.1: Validity of computational results for $-f''(0)$ with Khan and Mustafa [19]. When $M = 0$ and $K = 0$. 21
Table 2.2: Data of boundary stress and heat transmission computed from Eqs. (2.12) and (2.13) respectively, when $Pr = 10$ and $Ec = 0.5$. 21

Table 3.1: Comparison of bvp4c and shooting method for special case of Flat Plate $M = 0, Pr = 5, n = 0.5$. 32
Table 3.2: Comparison of bvp4c and shooting method for Newtonian Case $n = 0.5, Pr = 5$ and $K = 0$ 33

Abstract

This thesis describes boundary layer formations near a stretching cylinder placed in a shear-thinning fluid. An important Carreau fluid model is adopted to account for shear-thinning effects in the flow field. The thesis aims at discovering the significance of shear-thinning characteristic in the flow and thermal fields. Firstly, heat flow near an axially stretching cylinder immersed in Carreau fluid is formulated. Previous studies concerning Carreau fluid flow driven by a stretching cylinder are discussed with a view to point out some crucial errors concerning mathematical modeling. For computational results, a widely employed MATLAB package bvp4c is utilized, which is based on a collocation scheme. New numerical results of the resulting six parameter problem are worked out, which are utilized to assess the contribution of surface curvature on the flow fields in the presence of shear-thinning effect. In addition, plots of wall shear rates are elucidated for varying choices of parameters. Secondly, Mathematical modeling of flow around a stagnation-point on a vertical stretching cylinder is placed in a shear-thinning fluid is investigated. Buoyant force term arising due to the vertical boundary is formulated under the well-known Oberbeck-Boussinesq approximation. Numerical results are acquired using shooting technique via 5th order Runge-Kutta integration approach and additionally MATLAB built-in function bvp4c is applied to attest the solutions. Graphical illustrations are included to predict the contribution of buoyant force term on the underlying flow characteristics in the existence of non-Newtonian effect.

Chapter 1

Introduction

This chapter includes some fundamental definitions and preliminaries. Boundary layer flow and some associated dimensionless numbers used in this thesis are explained. Mathematical formulation for steady flow caused by axial stretching of a cylinder is discussed. A few models of shear-thinning/thickening fluids are also included.

1.1 Fundamental definitions

1.1.1 Compressible and incompressible flows

Incompressible flows are those flows where the fluid density remains consistent throughout the flow field. Most liquids are treated as incompressible fluids. On the other hand, flows where the density exhibits change either with respect to time or space variable are considered compressible. Flow of gases is generally regarded as compressible.

1.1.2 Steady and unsteady flows

Steady flow refers to the flow situation in which fluid properties such as velocity, volume, density, temperature and pressure do not exhibit variations with time. Whereas, in unsteady flow, at least any one of the fluid properties is time dependent.

1.1.3 Newtonian fluids

These fluids comply with the so-called Newton's law of viscosity, expressed below:

$$\tau_{yx} = \mu \frac{du}{dy}, \tag{1.1}$$

where τ_{yx} is shear stress in the x-direction, μ shows dynamic viscosity and du/dy shows the deformation rate for one-dimension and uni-direction flow above a plane surface. Commonly encountered Newtonian fluids are water and air.

1.1.4 Non-Newtonian fluids

For such fluids, the linear relationship between shear stress and strain rate does not. For such reason, the viscosity of non-Newtonian fluids changes with deformation rate. A broadly accepted and simple mathematical description of non-Newtonian behaviour is appended as follows:

$$\tau_{yx} = \lambda \left(\frac{du}{dy}\right)^{n}, \tag{1.2}$$

where, flow behavior index is denoted by n and λ designates consistency index.

Eq. (1.2) can also be written as:

$$\tau_{yx} = \eta \frac{du}{dy}. \tag{1.3}$$

In which $\eta = \lambda(du/dy)^{n-1}$ represents the apparent fluid viscosity.

Broad existence of non-Newtonian behavior in various industrial applications is obvious. Earlier researches have demonstrated that non-Newtonian fluid flow is useful in several industrial processes that includes, fluid drag reduction, surfactant applications for cooling/heating of huge buildings and utilization of polymer. Non-Newtonian behaviour is noted in mining and in biomedical industries. In the food processing industry, non-Newtonian characteristic of fluid is used for manufacturing of food products such as ketchup, mayonnaise and sauces etc.

Non-Newtonian fluids are classified as visco-elastic, time independent and time dependent in nature. Among the various categories of non-Newtonian fluids, visco-elastic fluids have degree of elasticity in addition to viscosity. Time-dependent fluids not only dependent upon the applied shear stress but also upon the time for which stress is being applied. Time independent fluids are also known as generalized Newtonian fluids. Viscosity of time independent fluids relies only on shear rate. Shear thinning, shear thickening and visco plastic fluids are the types of generalized Newtonian fluids. Different models have been presented to examine the properties of generalized Newtonian fluids due to their diverse fluid flow behaviors. The power law model is a widely adopted model which gives a simple relation between viscosity and shear rate. The other significant models are four-parameter models, namely, Carreau and Cross models which have been given considerable attention in the past.

1.1.5 Shear-thinning fluids/Shear-thickening fluids

Fluids that are shear-thinning or pseudoplastic have a decreasing apparent viscosity with increasing shear rate. These fluids include blood, certain paints, polymer solutions, and others. Shear thickening fluids or dilatants are those whose apparent viscosity rises with shear rate. Mixture of water and cornstarch is an example of shear-thickening fluid.

1.2 Mathematical models for shear-thinning/shear-thickening fluids

1.2.1 Power-law model

The power-law model is a widely employed model which gives a simple relation between viscosity and shear rate. Mathematically, apparent viscosity η is related with shear rate $\dot{\gamma}$ as follows:

$$\eta = \lambda(\dot{\gamma})^{n-1}, \tag{1.4}$$

where n is a positive number, known as power law index, λ is referred as consistency index. The response is shear-thinning fluid like $n < 1$, while for $n > 1$ signify shear-thickening character of the fluid. For $n = 1$, Eq. (1.4) collapses to the usual viscous fluid, in which η is constant. Power law model is applicable across a limited range of shear rates. As a result, the values of n and λ are determined by the range of shear rates considered.

1.2.2 Cross fluid model

In 1965, Cross introduced a four-parameter fluid model for shear-thinning/ shear-thickening fluids. The rheological equation of cross fluid model correlates viscosity and shear rate as follows:

$$\eta = \eta_\infty + \frac{\eta_0 - \eta_\infty}{1 + (\lambda|\dot{\gamma}|)^n}. \tag{1.5}$$

In which η_0 shows zero shear rate viscosity while η_∞ represents the infinite shear rate viscosity which is suitable for anticipating the behaviour of the material at high shearing situation. Flow behavior index is denoted by n while λ shows fluid relaxation time.

1.2.3 Carreau fluid model

In 1972, Pierre Carreau suggested the Carreau fluid model. This model relates apparent viscosity with shear rate as defined below:

$$\eta = \eta_\infty + (\eta_0 - \eta_\infty)[1 + (\lambda\dot{\gamma})^2]^{\frac{n-1}{2}}. \tag{1.6}$$

1.3 Boundary layer formation

When a fluid flows over a solid surface, it acquires a velocity almost equal to the velocity of solid surface. This velocity gradually changes from layer to layer. Fluid in contact with the solid surface

at rest has velocity equal to the wall velocity i.e. zero velocity, due to no-slip condition. The layer of fluid near the surface of solid where there is prominent effects of frictional force occurred is known as boundary layer. Outside boundary layer free stream velocity is maintained.

Like momentum boundary layer, when the ambient temperature and the temperature of the solid surface vary due to conduction or diffusion, thermal boundary layer develop. The fluid particles in contact with solid surface has the same temperature as the temperature of wall of solid surface. Energy transmits at the point where fluid particles are in contact with wall of solid is due to conduction. Then this energy flows between the layers of fluid and develop a temperature gradients. Thermal boundary layer is the region in fluid where these temperature gradients occur.

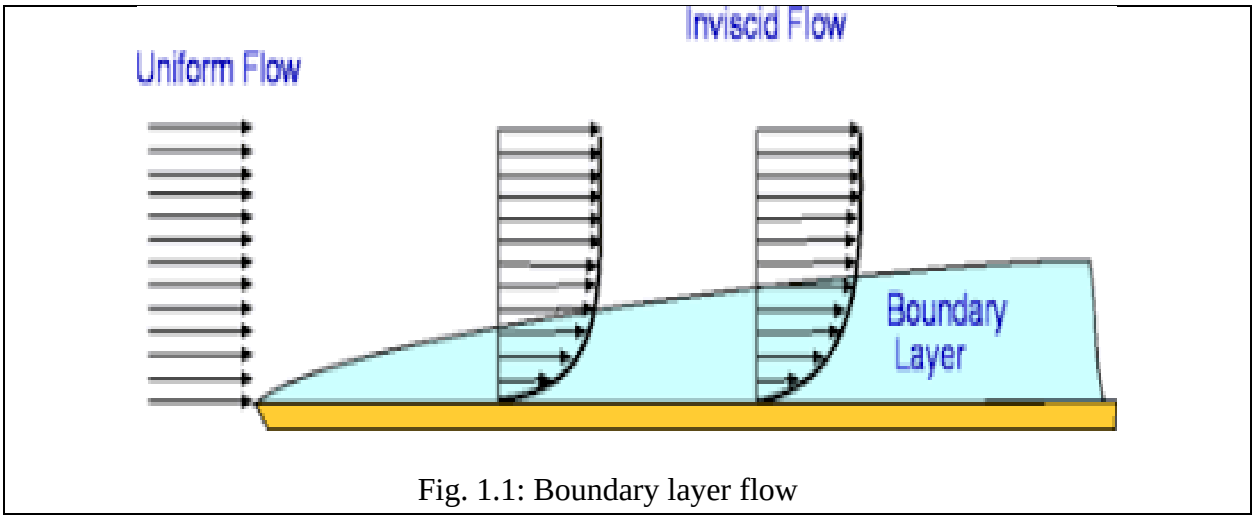

Fig. 1.1: Boundary layer flow

1.4 Some Dimensionless Numbers

1.4.1 Reynolds number

The ratio between inertial and viscous forces defines as Reynolds number. Mathematically, one can express:

$$Re = \frac{\text{inertial force}}{\text{viscous force}} = \frac{UL}{\nu}, \tag{1.7}$$

where L shows characteristic length, U denores the velocity and ν denotes the kinematic viscosity of the fluid. Reynolds number is used to classify laminar and turbulent flow situations of fluid. Viscous forces are dominant at low Reynolds numbers ($Re > 2000$), this causes laminar flow.

Inertial force becomes relatively dominant at a high Reynolds number ($Re > 4000$) creating turbulence in the fluid flow.

1.4.2 Prandtl number

Prandtl number gives a comparison of momentum and thermal diffusions in a flow field. It is used to calculate heat transfer between solid surface and moving fluid. Mathematically, we have

$$Pr = \frac{\mu C_p}{k}, \tag{1.8}$$

where k denotes thermal conductivity and C_p gives specific heat capacity.

1.4.3 Nusselt number

Nusselt number demonstrates the correlation between conduction and convection heat transfer. Mathematically, it is expressed as:

$$Nu = \frac{hL}{k}, \tag{1.9}$$

in which h denotes the convective heat transfer coefficient and k stands for thermal conductivity of fluid. Nusselt number measures the non-dimensional temperature gradient at the surface of solid.

1.4.4 Eckert number

The quotient of kinetic energy and enthalpy represents Eckert number. The number quantifies frictional heating phenomenon typically in high speed flows. Mathematically, it is expressed as:

$$Ec = \frac{kinetic\ energy}{enthalpy} = \frac{u^2}{C_p \Delta T}, \tag{1.10}$$

where u shows average velocity, C_p gives the specific heat capacity and ΔT designates the temperature difference.

1.5 Fluid flow over a stretching cylinder

Consider a two-dimensional steady flow of incompressible Newtonian fluid near a stretching cylinder. Source of flow is the axial stretching of an infinite cylinder which has velocity $u_0 x/L$,

in which u_0 is the characteristic velocity and L represents characteristic length. Here u and v represent velocity projections in the directions of axial (x) and radial (r) coordinates, respectively. The surface temperature of cylinder varies axially as $T_w = T_\infty + bx^2/L^2$, where T_∞ shows fluid ambient temperature and b is a positive constant with dimension $\{\theta\}$. The problem is governed by the following equation:

$$\frac{\partial}{\partial x}(ru) + \frac{\partial}{\partial r}(rv) = 0, \tag{1.11}$$

$$u\frac{\partial u}{\partial x} + v\frac{\partial u}{\partial r} = \nu\left(\frac{\partial}{\partial r} + \frac{1}{r}\right)\frac{\partial u}{\partial r}, \tag{1.12}$$

$$\rho c_p\left(u\frac{\partial T}{\partial x} + v\frac{\partial T}{\partial r}\right) = k\left(\frac{\partial}{\partial r} + \frac{1}{r}\right)\frac{\partial T}{\partial r}. \tag{1.13}$$

Eqs. (1.11)- (1.13) are to be solved subject to the following conditions:

$$u(x,R) = u_w(x) = \frac{u_0 x}{L}, \qquad v(x,R) = 0, \qquad T(x,R) = T_w = T_\infty + \frac{bx^2}{L^2}, \tag{1.14}$$
$$u \to 0, \quad T \to T_\infty \quad \text{as} \quad r \to \infty.$$

In Eqs. (1.11)- (1.14), $\nu = \mu/\rho$ denotes the kinematic viscosity of fluid, ρC_p represents the effective heat capacity while k is the thermal conductivity of fluid under consideration.

To convert Eqs. (1.11)- (1.13) into ODEs, following similarity transformation variables are used:

$$\psi(x,r) = \sqrt{u_w \nu x}\, R f(\eta), \qquad \eta = \frac{r^2 - R^2}{2R}\left(\frac{u_0}{L\nu}\right)^{\frac{1}{2}}, \qquad \theta(\eta) = \frac{T - T_\infty}{T_w - T_\infty}. \tag{1.15}$$

Where $\psi(x,r)$ is axisymmetric stream function, similarity variable is denoted by η and $\theta(\eta)$ gives non-dimensional temperature. It is easy to verify that the use of transformation (1.15) in Eqs. (1.12) and (1.13) lead us to the following equations:

$$(1 + 2M\eta)f''' + 2Mf'' + ff'' - f'^2 = 0, \tag{1.16}$$

$$\frac{1}{Pr}\{(1 + 2M\eta)\theta'' + 2M\theta'\} + f\theta' - 2f'\theta = 0. \tag{1.17}$$

$$f(0) = 0, \qquad f'(0) = 1, \qquad \theta(0) = 1,$$
$$f' \to 0, \qquad \theta \to 0 \quad \text{as} \quad \eta \to \infty. \tag{1.18}$$

In above equations, $M = (\nu L/R^2 u_0)^{1/2}$ denotes the curvature parameter and $Pr = \mu C_p/k$ shows Prandtl number. With the aid of MATLAB built-in routine bvp4c, a few graphical results are shown in Figs. 1.2(a) and 1.2(b).

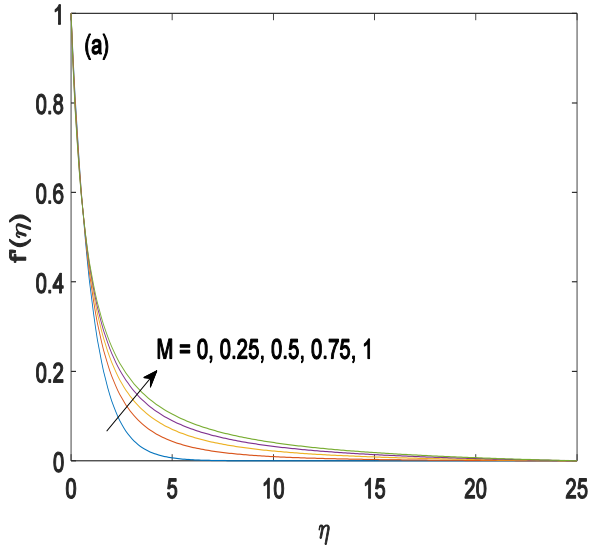

Fig 1.2 (a): Axial velocity curves at various values of M when $Pr = 5$.

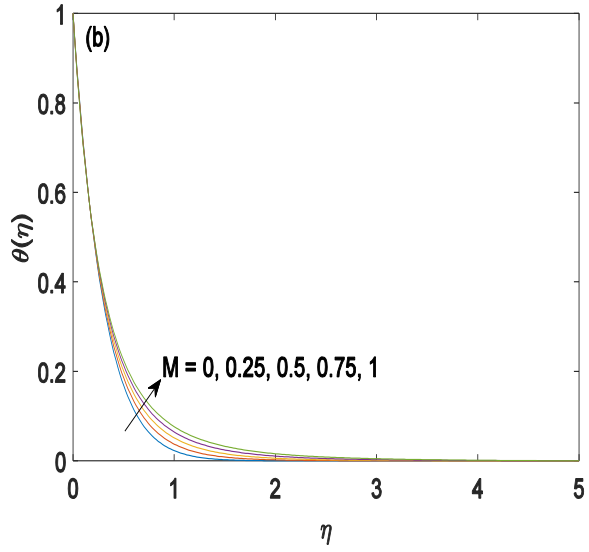

Fig 1.2 (b): Dimensionless temperature $\theta(\eta)$ for a variety of M values when $Pr = 5$.

1.6 Heat transfer

Heat transfer takes places between physical systems as a result of temperature gradient. Flow of heat occurs from a region of higher temperature to a region lower temperature.

1.6.1 Conduction

Conduction is a process of heat transfer which occurs due to the collision of molecules in a medium. As a result of Molecules with higher kinetic energy colliding with molecules having lower kinetic energy, lower kinetic energy molecules obtain energy. Hence, energy transfer in conduction is due to interaction of molecules in a medium. This conduction is also known as heat

conduction. Heat conduction, electrical conduction, and sound conduction are all terms that are frequently used to describe three different types of activity. Heat conduction relies on the temperature gradient, cross section area of material and physical properties. The rate of conduction is calculated as follows:

$$Q = \frac{k.A(T_{hot} - T_{cold})}{d}, \tag{1.19}$$

in which k represents thermal conductivity, A is the area, d denotes thickness of body, T_{hot} and T_{cold} are temperatures of hot region and cold regions respectively.

1.6.2 Convection

Convection is defined as the flow of fluid molecules from higher to lower thermal energy regions. Heat convection takes place due the density difference of fluid molecules in the region. As the temperature increases volume of fluid molecules also increases, hence the density of molecules decreases. This causes displacement of molecules. Newton's law of cooling has given Heat Transmission phenomenon as below:

$$Q = h.A\left(T_w - T_f\right), \tag{1.20}$$

Where h denotes heat transfer coefficient. T_w is the wall temperature and $T_f$is surrounding temperature.

1.6.3 Radiation

In the infrared and visible regions of the electromagnetic spectrum, radiation is the transmission of thermal energy carried by photons of light. Radiation is a mechanism by which all bodies constantly emit thermal energy. It can be sent without the use of any medium.

1.7 Literature review

It is widely acknowledged that most of the fluids treated in industrial processes are non-Newtonian, that is viscosity of such fluids depends on the flow conditions such as shear rate, flow geometry etc. Common examples are industrial fluids (paints, ceramic, motor oil, etc.), biological fluids (blood, semen, saliva, etc.), geophysical flows (magma, lava, ice, etc.) and fluids encountered in chemical engineering such as polymeric liquids, silicon oils etc. In one of the categories of non-

Newtonian materials, viscosity changes with varying deformation rate. Various models of such fluids are available in the literature. A famous power-law model (presented by Ostwald-de-Waele [1]) has been the most preferred model apparently because of its simplicity. It's a two-parameter model that is only suitable for a small range of shear rates. Moreover, power law model is unable to predict fluid viscosity at zero and infinite shear rate rates. Other significant generalized Newtonian models are the four parameter models suggested by Cross [2] and Carreau [3] which are valid over wide range of shear rate. In the past, Carreau fluid model had been extensively used to formulate a variety of flow situations. These include peristaltic flow problems in both planar and curved channels [4], [5], [6], [7], [8], classical von-Karman problem of infinite rotating disk [9], [10], [11] and boundary layer flows around flat surfaces [12], [13], [14], [15] just to refer a few of them.

Boundary layer formation near flat or curved extendable surfaces in the existence of magnetic field has special essence in modern metallurgical applications. Also, heat transfer in fluid flows has abundant applications in heat exchangers, energy production, space cooling, cooling towers and many others. Problem of laminar flow produced by stretching of a cylinder in a viscous fluid with heat transfer was firstly investigated by Wang [16] using similarity analysis. After this pioneering study, several researchers explored this problem under different physical features such as partial slip considerations [17], [18], [19], buoyancy force effects [20], time-dependent stretching wall velocity consideration [21], [22], [23], [24], heat transfer with entropy generation [25], Joule heating and viscous dissipation in Casson liquid [26] and non-uniform cylinder radius consideration [27]. Heat transfer problem for laminar flow around a cylindrical surface subjected to magnetic field was attempted by Ishak et al [28]. Kumar et al. [29] used a numerical scheme to discuss heat/mass transport phenomena in a hybrid nanofluid flowing over a stretchable cylinder with a magnetic dipole. Wang's framework has also been explored using Carreau or Cross fluid models. For instance, reader is referred to the articles published by Salahuddin et al [30], Hashim et al. [31], Khan et al. [32] and Iqbal et al. [33]. However, the local similarity equations obtained in these papers are not error free, which will be discussed later.

Stagnation-point flows have received broader attention in past due to its relevant industrial and engineering applications. It helps in design of thrust bearings and radial diffusers, friction reduction, transpiration cooling, polymer processing, as well as in aerodynamics. Hiemenz [34]

discovered a planar stagnation-point flow on a solid surface held stationary in a viscous fluid. Mahapatra et al. [35] published an interesting study describing fluid motion adjacent to a stagnation-point on a linearly deforming surface using numerical solution. Mustafa et al. [36] solved a non-linear heat transmission problem for stagnation-point flow involving power-law fluids. Power-law fluid impinging on a flat surface stretching with non-linearly varying velocity was investigated by Layek et al. [37] using Lie symmetry analysis. Dholey [38] analyzed unsteady two-dimensional stagnation-point flow near a moving plate which is placed in non-Newtonian fluid obeying power-law model. Xie and Wang [39] discussed heat transmission in a power law fluid flowing over a stretchable surface containing a stagnation-point. Similar stagnation-point flows in light of Carreau model have also been reported in some studies ([40], [41], [42]).

The current thesis has two objectives. Firstly, to formulate heat transfer occurring near an axially stretchable cylinder immersed in a Carreau fluid. Our intention is to present new local similarity equations of momentum and heat transfer problems. Moreover, energy equation containing viscous dissipation and Joule heating terms is solved numerically for broad parameter values. Numerical simulations are executed via MATLAB routine bvp4c. To preserve self-similarity in the system variable surface temperature of cylinder is considered. Furthermore, the famous Oberbeck-Boussinesq simplification is used to formulate the buoyant force term. By using the shooting method via the 5th order RK integration approach, governing equations are numerically solved.

Chapter 2

Novel numerical results for heat transfer along a stretching cylinder immersed in a shear-thinning fluid

2.1 Introduction

This chapter discusses boundary layer development around a cylinder stretching axially in a shear-thinning fluid obeying Carreau model. Heat transfer problem is examined in the existence of frictional heating and Joule heating terms in the thermal energy equation. After. MATLAB built-in routine bvp4c is used to generate computational results.

2.2 Problem formulation

Consider a steady-state two-dimensional flow situation which arises if an infinite cylinder of radius R stretches axially in a constant density shear-thinning fluid, which would otherwise be at rest. A well-known Carreau model will be utilized to account for the shear-thinning characteristic in the flow field. The cylinder stretches with the velocity $u_w = u_0 x/L$, where u_0 shows characteristic velocity and L the characteristic length (see Fig. 2.1). Let u and v represent velocities in the $x-$ and $r-$ directions respectively where x is the axial coordinate and r is normal to it. It will be shown later that self-similar analysis is perceivable only if the cylindrical surface is kept at a prescribed temperature of the form $T_w = T_\infty + bx^2/L^2$, where T_∞ shows the ambient temperature and $b > 0$ is a constant. Fluid flow is supposed to be influenced by transverse magnetic field of intensity B_0 in the radial direction, and this yields a Lorentz force with components $F_B = [-\sigma B_0^2 u, 0, 0]$ where σ stands for electrical conductivity. The analysis will be made in the existence of frictional heating and Joule heating terms. Carreau [3] proposed following form of apparent viscosity for shear-thinning fluids:

$$\eta = \eta_\infty + (\eta_0 - \eta_\infty)[1 + (\lambda\dot{\gamma})^2]^{\frac{n-1}{2}}, \tag{2.1}$$

where η_∞ and η_0 represent infinite and zero shear rate viscosities, λ is a material constant which has dimension $\{T\}$, n is labelled as flow behavior index which can assume values in the range $0 \leq n \leq 1$. For the sake of simplicity, in finite shear viscosity η_∞ shall be ignored. Model suggests that

fluid viscosity remains consistent at low shear rates ($\dot{\gamma} \ll 1/\lambda$) and viscosity decreases (approximately linearly) with increasing shear rate at high shear rates ($\dot{\gamma} \gg 1/\lambda$). Notice that the transition from the constant viscosity to the shear thinning behavior occurs when $\lambda\dot{\gamma} = 1$.

The shear-rate $\dot{\gamma}$ in Eq. (2.1) is defined as follows:

$$\dot{\gamma} = \left\{2\left(\frac{\partial v}{\partial r}\right)^2 + 2\left(\frac{v}{r}\right)^2 + 2\left(\frac{\partial u}{\partial x}\right)^2 + \left(\frac{\partial u}{\partial r} + \frac{\partial v}{\partial x}\right)^2\right\}^{1/2}. \tag{2.2}$$

In view of Eqs. (2.1) and (2.2), aforesaid problem under boundary layer approximations is described via following PDEs (see, for instance, Ref. [31]):

$$\frac{\partial}{\partial x}(ru) + \frac{\partial}{\partial r}(rv) = 0, \tag{2.3}$$

$$u\frac{\partial u}{\partial x} + v\frac{\partial u}{\partial r} = \nu\left(\frac{\partial}{\partial r} + \frac{1}{r}\right)\left[\left(\frac{\partial u}{\partial r}\right)\{1 + (\lambda\dot{\gamma})^2\}^{\frac{n-1}{2}}\right] - \frac{\sigma}{\rho}B_0^2 u, \tag{2.4}$$

$$\rho c_p\left(u\frac{\partial T}{\partial x} + v\frac{\partial T}{\partial r}\right) = k\left(\frac{\partial^2 T}{\partial r^2} + \frac{1}{r}\frac{\partial T}{\partial r}\right) + \eta_0\{1 + (\lambda\dot{\gamma})^2\}^{\frac{n-1}{2}}\left(\frac{\partial u}{\partial r}\right)^2 + \sigma B_0^2 u^2, \tag{2.5}$$

where $\nu = \eta_0/\rho$ defines kinematic viscosity at zero shear rate, c_p designates specific heat capacity at constant pressure and k represents thermal conductivity. Last two terms in Eq. (2.5) appear due to the consideration of frictional heating and Joule heating effects.

Invoking no-slip assumption, boundary conditions are posed as follows:

$$\begin{gathered} u(x,R) = u_w(x) = \frac{u_0 x}{L},\ \ v(x,R) = 0,\ \ T(x,R) = T_w = T_\infty + \frac{bx^2}{L^2}, \\ u \to 0,\quad T \to T_\infty \quad \text{as} \quad r \to \infty. \end{gathered} \tag{2.6}$$

To investigate the solution of Eqs. (2.3)-(2.5), following similarity transformation variables are used [31]:

$$\psi(x,r) = (u_w \nu x)^{1/2} R f(\eta),\ \ \eta = \frac{r^2 - R^2}{2R}\left(\frac{u_0}{L\nu}\right)^{\frac{1}{2}},\ \ \theta(\eta) = \frac{T - T_\infty}{T_w - T_\infty}, \tag{2.7}$$

where η is the similarity variable, ψ denotes axisymmetric stream function which is defined as $u = r^{-1}\psi_r$ and $v = -r^{-1}\psi_x$ and $\theta(\eta)$ defines the dimensionless temperature field. Using Eq. (2.7), Eqs. (2.4) and (2.5) and the boundary conditions (2.6) are transformed as follows:

$$f''' + \frac{\left\{2(1+\Lambda)^{\frac{n-1}{2}} + (n-1)\Lambda(1+\Lambda)^{\frac{n-3}{2}}\right\} Mf'' + ff'' - Ha^2 f' - f'^2}{\left((1+\Lambda)^{\frac{n-1}{2}} + (n-1)\Lambda(1+\Lambda)^{\frac{n-3}{2}}\right)(1+2M\eta)} = 0, \tag{2.8}$$

$$\begin{aligned} &\frac{1}{Pr}\{(1+2M\eta)\theta'' + 2M\theta'\} + f\theta' - 2f'\theta \\ &\qquad + Ec\left\{(1+2M\eta)(1+\Lambda)^{\frac{n-1}{2}} f''^2 + Ha^2 f'^2\right\} = 0, \end{aligned} \tag{2.9}$$

where $\Lambda = (1+2M\eta)K^2 f''^2$.

$$\begin{aligned} f(0) = 0,\ \ f'(0) = 1,\ \ \theta(0) = 1, \\ f' \to 0,\ \ \theta \to 0 \quad \text{as} \quad \eta \to \infty. \end{aligned} \tag{2.10}$$

In Eqs. (2.8) and (2.9), $M = (\nu L/u_0 R^2)^{1/2}$ is named curvature parameter, $K = (\lambda u_0/L)Re_x^{1/2}$ is termed as local Weissenberg number in which $Re_x = u_w x/\nu$ defines the local Reynolds number, $Ha = (\sigma B_0^2 L/\rho u_0)^{1/2}$ defines the Magnetic interaction parameter, $Pr = \eta_0 c_p/k$ designates Prandtl number and $Ec = u_w^2/c_p(T_w - T_\infty)$ defines the constant Eckert number.

Presence of the term $(1+2M\eta)$ in the expression of Weissenberg number defined in refs. [31], [32] and [33] was overlooked by the authors. It is clear from the factor (r^2/R^2) in Weissenberg number defined in refs. [31]-[33]. That is why, some terms involving $(1+2M\eta)$ are missed in the refs. [31]-[33].

Local skin friction coefficient C_f is defined as follows:

$$C_f = \frac{\tau_{xr}|_{r=R}}{\rho u_w^2} = \eta_0 \left(\frac{\partial u}{\partial r}\right)\left\{1 + \left(\lambda\left(\frac{\partial u}{\partial r}\right)\right)^2\right\}^{\frac{n-1}{2}}\Bigg|_{r=R} / \rho u_w^2. \tag{2.11}$$

In view of Eq. (2.7), Eq. (2.11) reduces to the following form:

$$Re_x^{\frac{1}{2}}\ C_f = f''(0)\{1 + (K(f''(0))^2\}^{\frac{n-1}{2}}. \tag{2.12}$$

Another parameter of engineering significance is the local Nusselt number evaluated as below:

$$Nu_x = -\frac{x(\partial T/\partial r)_{r=R}}{(T_w - T_\infty)} = -Re_x^{\frac{1}{2}}\theta'(0). \tag{2.13}$$

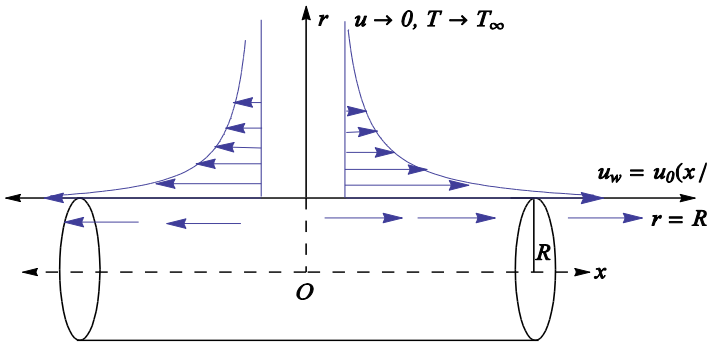

Fig. 2.1: A schematic of fluid flow over a cylindrical surface

2.3 Some particular cases

2.3.1 Flat surface case

When $M = 0$ or $R \to \infty$, Eqs. (2.8) and (2.9) represent momentum and heat transfer in Carreau fluid flow along a stretching surface. For such problem, Eqs. (2.8) and (2.9) reduce to:

$$f''' + \frac{ff'' - Ha^2 f' - f'^2}{(1 + K^2 f''^2)^{\frac{n-1}{2}} + (n-1)(K^2 f''^2)(1 + K^2 f''^2)^{\frac{n-3}{2}}} = 0, \tag{2.15}$$

$$\frac{1}{Pr}\theta'' + f\theta' - 2f'\theta + Ec\left\{\left(1 + K^2 f''^2\right)^{\frac{n-1}{2}} f''^2 + Ha^2 f'^2\right\} = 0, \tag{2.16}$$

with the same boundary conditions (2.10).

2.3.2 Case of Newtonian fluid

For $K = 0$, the governing equations (2.8) and (2.9) collapse to the non-Newtonian fluid case. In this case, Eqs. (2.8) and (2.9) acquire the following forms:

$$(1 + 2M\eta)f''' + 2Mf'' + ff'' - Ha^2 f' - f'^2 = 0, \tag{2.17}$$

$$\frac{1}{Pr}\{(1 + 2M\eta)\theta'' + 2M\theta'\} + f\theta' - 2f'\theta + Ec\{(1 + 2M\eta)f''^2 + Ha^2 f'^2\} = 0. \tag{2.18}$$

Subject to the same conditions (2.10).

2.4 Method of solution

The governing problem represented by Eqs. (2.8) and (2.9) is strongly non-linear whose exact solution appears very difficult. Hence, Eqs. (2.8) and (2.9) along with the conditions (2.10) have been dealt numerically by a simple yet effective package bvp4c of the software MATLAB. For this package, the equivalent first-order system is required, which is derived by making the following substitutions:

$$Y_1 = f,\ \ Y_2 = f',\ \ Y_3 = f'',\ \ Y_4 = \theta,\ \ Y_5 = \theta'. \tag{2.19}$$

A following system comprising five first-order equations is retrieved:

$$Y_1{}' = Y_2, \tag{2.20}$$

$$Y_2{}' = Y_3, \tag{2.21}$$

$$Y_3{}' = -\frac{\left\{2(1+\Lambda)^{\frac{n-1}{2}} + (n-1)\Lambda(1+\Lambda)^{\frac{n-3}{2}}\right\}MY_3 - Ha^2Y_2 - Y_2^2 + Y_1Y_3}{\left\{(1+\Lambda)^{\frac{n-1}{2}} + (n-1)\Lambda(1+\Lambda)^{\frac{n-3}{2}}\right\}(1+2M\eta)}, \tag{2.22}$$

$$Y_4' = Y_5, \tag{2.23}$$

$$Y_5' = -\frac{2MY_5 + Pr\left\{Y_1Y_5 - 2Y_2Y_4 + Ec\left\{(1+2M\eta)(1+\Lambda)^{\frac{n-1}{2}}Y_3^2 + Ha^2Y_2^2\right\}\right\}}{(1+2M\eta)}. \tag{2.24}$$

Eqs. (2.22) and (2.24) along with the boundary conditions (2.10) are expressed in MATLAB code bvp4c. The code is executed in a smaller domain $[0, L]$ at first, and then the value of L is gradually increased while initial slopes $f''(0)$ and $\theta'(0)$ are computed at all chosen values of L. Our computations have indicated that the value of $L = 20$ was found to fulfill a threshold value of 10^{-6} for functions $Y_2(\infty)$ and $Y_4(\infty)$.

2.5 Numerical results and discussion

Numerical approximations have been developed for varying values of different parameters which include curvature parameter M, magnetic interaction parameter Ha, flow behavior index n, local Weissenberg number K, Prandtl number Pr and Eckert number Ec. For illustration of computational results, graphs of velocity components and temperature are plotted against η in the figures. The changes in velocity components u and v, represented by f' and f respectively are demonstrated by changing curvature parameter M is shown in Fig. 2.2(a). Radial flow enhances while axial flow weakens as distance from the wall is increased. Fluid flow is seen to accelerate in

both directions whenever curvature effects are incremented. Moreover, stream wise diffusion of momentum grows considerably for increasingly higher values of M. As parameter M enlarges, relative significance of heat conduction term $(1 + 2M\eta)\theta'' + 2M\theta'$ improves and, consequently, stream wise thermal diffusion is greatly enhanced (as evident through Fig. 2.2 (b)).

Next, the contribution of Lorentz force term on the velocity components and temperature profile is discussed in Figs. 2.3(a) and 2.3(b). In this regard, graphs for f, f' and θ versus η are generated for different choices of parameter Ha measuring the strength of Lorentz force. For increasing Ha-values, Lorentz force gives more opposition to the near wall fluid which decelerates the axially directed flow. Radial flow adjacent to the cylinder is accordingly reduced, as apparent from Fig. 2.3(a). In addition, more heat generation is anticipated due to the strengthening of Joule heating effect which is caused by an increment in Ha. For such reason, a growing trend in thermal penetration depth is witnessed whenever magnetic field is imposed (see Fig. 2.3(b)).

Graphical representations of velocity and temperature fields under the effect of flow behavior index n are provided in Figs.2. 4(a) and 2.4(b). As parameter n grows, apparent viscosity function given by Eq. (2.1) enlarges which thereby favors the stream wise momentum diffusion. It is reflected from the graphs of f or f' in Fig. 2.4(a), which move away from the wall signaling a growth in boundary layer thickness. On the other hand, heat conduction effect intensifies with increasing n as noted from Fig. 2.4 (b).

To foresee how Weissenberg number K influences the flow fields, computed graphs of f and f' versus η are presented in Fig.2.5(a) for varying choices of K. For larger values of K, fluid relaxation time is higher due to which boundary layer thickness does not develop as fast as for a fluid with a relatively smaller relaxation time. Such tendency is apparent from the graphical results in Fig. 2.5a. Fig. 2.5(b) determines the contribution of Prandtl number Pr on the accompanying heat transfer phenomenon. By increasing Pr, the significance of heat convection term increases which weakens heat conduction due to which thermal boundary layer suppresses.

The influence of Eckert number Ec on temperature curves can be determined from Fig. 2.6. Fluid temperature goes up as the value of Ec increases, as shown in the graph. The ratio of kinetic energy to the enthalpy defines Eckert number. This leads to an enhanced temperature profile as shown in Fig. 2.6.

Plots of skin friction factor and local Nusselt number against flow behavior index n are derived for different M-values (see Figs. 2.7(a) and 2.7(b)). Growth in resisting force with increasing n is approximately linear for sufficiently smaller values of M. Qualitatively speaking, variation in $\theta'(0)$ with n is similar to the graph of $f''(0)$ versus n at all choices of M.

Expressions given by Eqs. (2.12) and (2.13) have been utilized to compute skin friction coefficient and local Nusselt number. In table 2.1, results of $f''(0)$ are compared with those computed by previous studies in a special case. Our results are found to be consistent with those of [19] and [26] for all considered values of parameter Ha. Table 2.2 shows that resisting force on the cylindrical surface enlarges for increasing values of n. Moreover, heat transport from the solid wall also improves upon consideration of shear-thinning effects. It is also reflected that lesser force is needed to displace a fluid on a surface which has a higher relaxation time. Heat transport from the solid wall also deteriorates for increasing stress relaxation effects. In addition, a substantial rise/reduction in resisting force/heat transfer rate is anticipated whenever magnetic field effects are incorporated.

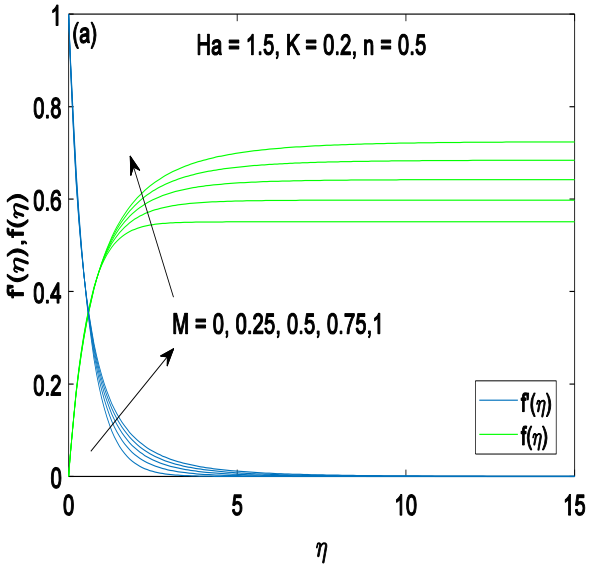

Fig. 2.2 (a): Distribution of axial velocity field for various choices of curvature parameter M.

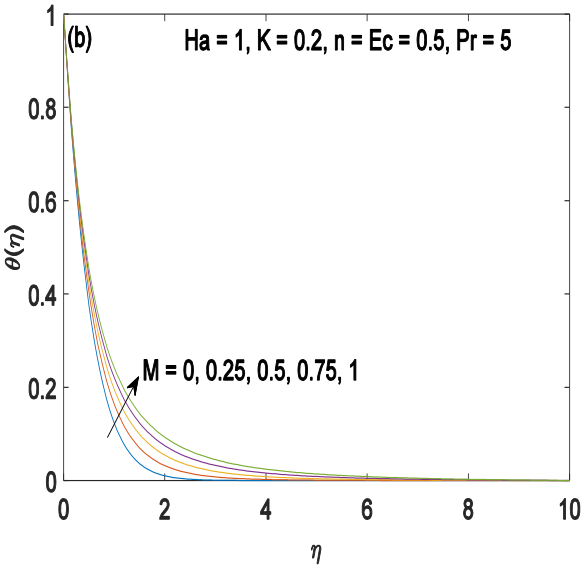

Fig. 2.2 (b): Distribution of temperature field for various choices of curvature parameter M.

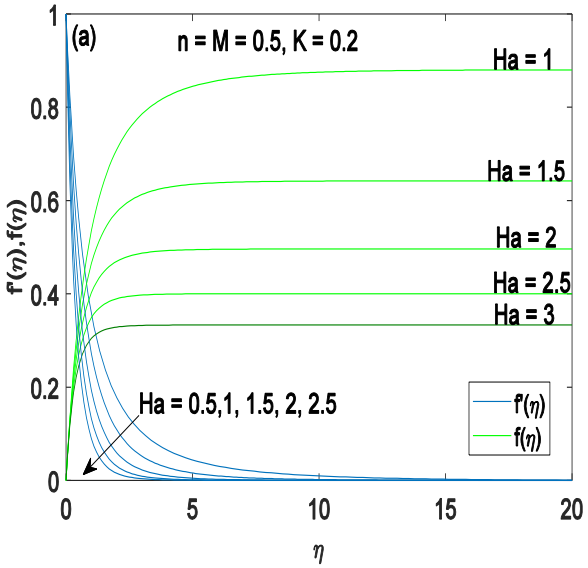

Fig. 2.3 (a): Distribution of axial velocity field for various choices of magnetic interaction parameter Ha.

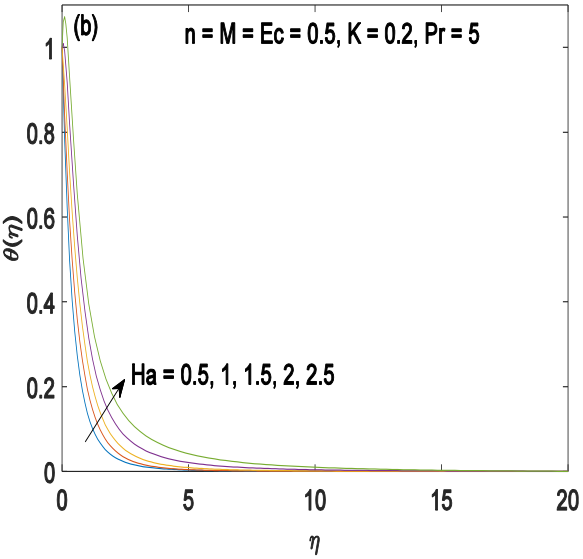

Fig. 2.3 (b): Distribution of temperature field for various choices of magnetic interaction parameter Ha.

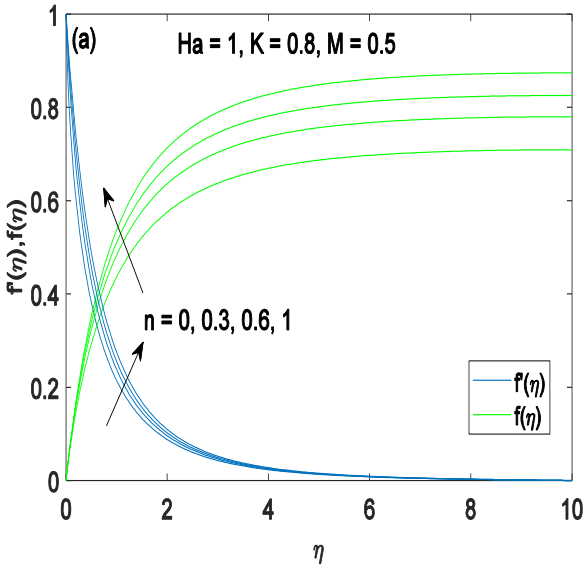

Fig. 2.4 (a): Distribution of axial velocity field For various choices of flow index behavior n.

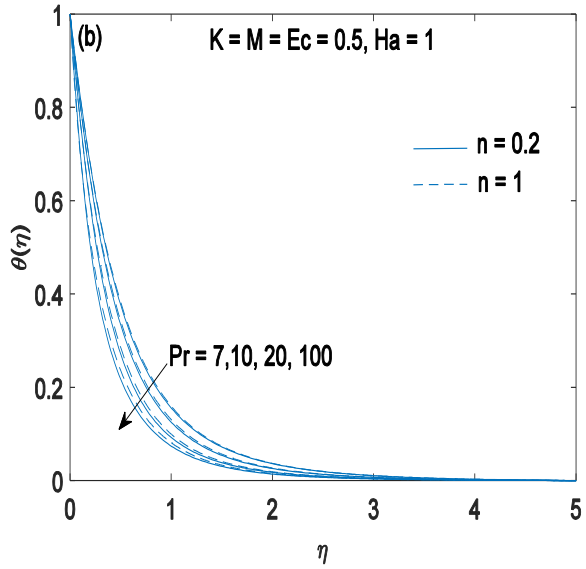

Fig. 2.4 (b): Distribution of temperature field for various choices of flow index behavior n.

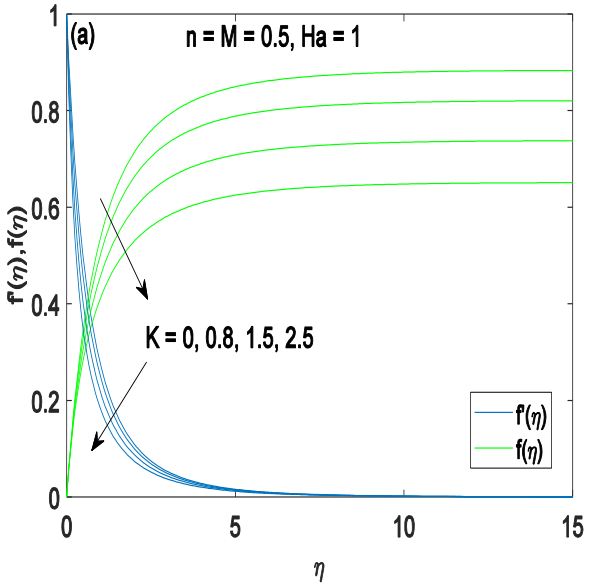

Fig. 2.5 (a): Distribution of axial velocity field for various choices of local Weissenberg number K.

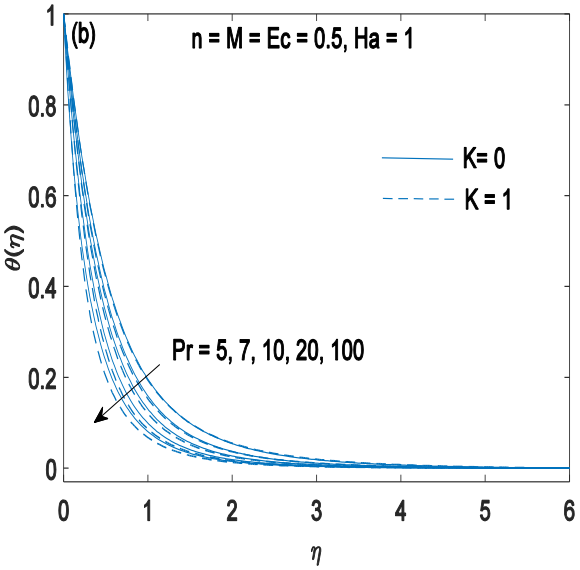

Fig. 2.5 (b): Distribution of temperature field for various choices of local Weissenberg number K.

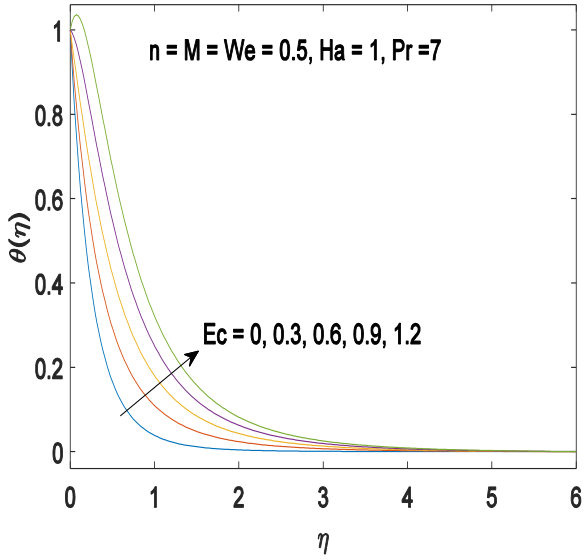

Fig 2.6: Variation of temperature θ with η by changing Eckert number values.

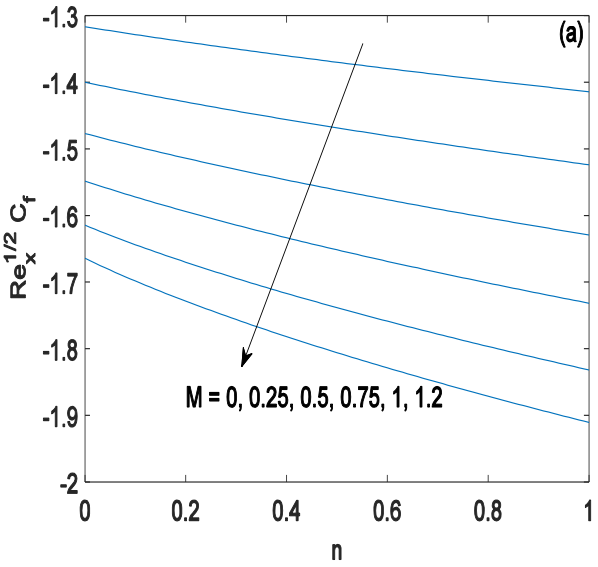

Fig. 2.7 (a): Variation in skin friction coefficient for different values of curvatutre parameter M.

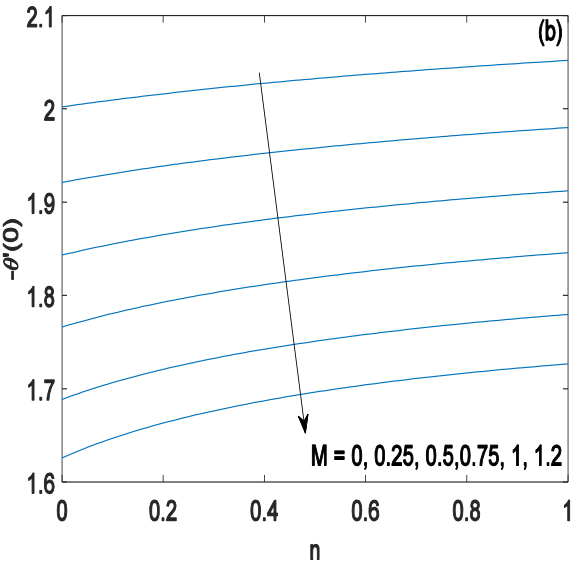

Fig. 2.7 (b): Variation in Nussselt number for different values of curvatutre parameter M.

Table 2.1: Validity of computational results for $-f''(0)$ with Khan and Mustafa [19]. When $M = 0$ and $K = 0$.

	$-f''(0)$		
Ha	Tamoor et. al. [26]	Khan and Mustafa [19]	Present
0	1	1	1
0.2	1.01980	1.0198039	1.019803894
0.5	1.11803	1.118034	1.118033987
0.8	1.28063	1.2806248	1.280624844
1	1.41421	1.4142136	1.414213561

Table 2.2: Data of boundary stress and heat transmission computed from Eqs. (2.12) and (2.13) respectively, when $Pr = 10$ and $Ec = 0.5$.

n	K	M	Ha	$Re_x^{1/2} C_f$	$Re_x^{-1/2} Nu_x$
0.2	0.5	0.5	1	-1.51210	2.07393
0.5				-1.55956	2.10493
0.8				-1.60110	2.12685
1				-1.62649	2.13833
0.7	0.3	0.5	1	-1.61131	2.13078
	0.7			-1.55865	2.10949
	1			-1.51237	2.09758
	1.5			-1.44164	2.09155
0.7	0.5	0	1	-1.38851	2.34877
		0.3		-1.51082	2.20708
		0.6		-1.62513	2.07859
		1		-1.76846	1.92065
0.7	0.5	0.5	1.2	-1.73060	1.47842
			1.5	-1.95778	0.40436
			2	-2.35372	-1.60101

2.6 Concluding remarks

A numerical solution is found for steady flow around a stretching cylinder in a shear-thinning fluid. Earlier analysis in this direction were made via incorrect formulations of the transport equations. This study presents new formulations of the governing local similarity equations. Obtained numerical solution has enabled us to identify the curvature and shear-thinning effects on the underlying flow physics. Noteworthy observations of this research are summarized below:

- Compared with the Newtonian fluid case, Carreau fluid assumption results in two additional parameters in the problem namely flow behavior index n and Weissenberg number K.

- Contribution of parameter n is such that the stream-wise momentum diffusion grows for increasing values of n. Moreover, a slight enhancement in thermal diffusion is also detected whenever shear-thinning effects are incorporated.
- For rising Weissenberg number K, fluid relaxation time grows due to which momentum boundary layer shrinks.
- As curvature parameter M becomes large, fluid flow accelerates in both radial and axial directions. Moreover, parameter M is multiplied with the terms θ'' and θ' which quantify heat conduction effect. Therefore, heat conduction effect is elevated whenever M is incremented.
- Momentum diffusion is significantly reduced in the presence of magnetic field compared with the case of no magnetic field.

Chapter 3

Mathematical modeling of stagnation-point flow impinging on a stretching vertical cylinder in Carreau fluid with heat transfer

3.1 Introduction

In this chapter, Mathematical modeling of flow around a stagnation point on a vertical stretching cylinder placed in a shear-thinning fluid is studied. An important Carreau fluid model is adopted to account for shear-thinning effects in the flow field. To retain a self-similar analysis of the model, variable surface temperature is considered. Locally similar solutions are obtained using usual transformation.

3.2 Basic equations and problem formulation

Stagnation-point flow of generalized Newtonian fluid obeying Carreau model along a vertical stretchable cylinder is considered. u and v represent velocity projections in the directions of axial (x) and radial (r) coordinates, respectively, where x is held along the cylinder axis and r is normal to it. It is presumed that the cylinder boundary expands axially with a velocity $u_0 x/L$, where u_0 defines characteristic velocity and L represents characteristic length. The external flow is denoted by $u_e(x) = u_1 x/L$ and $v_e(r) = -u_1 r/2L$. The velocity of external flow is defined as,$u_e(x) = u_1 x/L$, where $u_1 > 0$ is reference velocity. The cylindrical surface is maintained at a prescribed temperature of the form $T_w = T_\infty + bx/L$, where b is a constant. Using small magnetic Reynolds number assumption which allows to neglect induced magnetic field and assuming further that imposed and induced electric fields are absent due to polarization of charges, the components of Lorentz force vector simplify to $F_x = -\sigma B_0^2 u$ and $F_r = 0$. Buoyant force term is formulated using Oberbeck-Boussinesq approximation, according to which density difference can be neglected everywhere except where density is multiplied with g where, g is gravitational acceleration. Accounting the assumptions, governing equations under boundary layer approximations are presented below:

$$\frac{\partial}{\partial x}(ru) + \frac{\partial}{\partial r}(rv) = 0, \tag{3.1}$$

$$u\frac{\partial u}{\partial x}+v\frac{\partial u}{\partial r}=u_e\frac{du_e}{dx}+\nu\left(\frac{\partial}{\partial r}+\frac{1}{r}\right)\left[\left(\frac{\partial u}{\partial r}\right)\{1+(\lambda\dot{\gamma})^2\}^{\frac{n-1}{2}}\right]+g\beta(T-T_\infty)-\frac{\sigma}{\rho}B_0^2(u-u_e), \tag{3.2}$$

$$\rho c_p\left(u\frac{\partial T}{\partial x}+v\frac{\partial T}{\partial r}\right)=k\left(\frac{\partial^2 T}{\partial r^2}+\frac{1}{r}\frac{\partial T}{\partial r}\right). \tag{3.3}$$

It is assumed that there is no surface slip and permeability effects. This result in the following boundary conditions:

$$u(x,R)=u_w(x)=\frac{u_0 x}{L},\ \ v(x,R)=0,\ \ T(x,R)=T_w=T_\infty+\frac{bx}{L},$$
$$u\to u_e(x)=\frac{u_1 x}{L},\ \ v\to v_e(r)=-\frac{u_1 r}{2L},\ \ T\to T_\infty\ \text{ as }\ r\to\infty. \tag{3.4}$$

In Eqs. (3.2-3.3), ρ stands for fluid density, $\nu=\eta_0/\rho$ defines the kinematic viscosity, σ designates electrical conductivity of the fluid, the thermal conductivity of fluid is expressed as k, C_p expresses specific heat capacity and β stands for thermal expansion coefficient.

To find a similarity solution of Eqs. (3.1-3.3) subject to the boundary conditions (3.4), following substitutions are introduced:

$$\psi(x,r)=\sqrt{u_w\nu x}Rf(\eta),\ \ \eta=\frac{r^2-R^2}{2R}\left(\frac{u_0}{L\nu}\right)^{\frac{1}{2}},\ \ \theta(\eta)=\frac{T-T_\infty}{T_w-T_\infty}. \tag{3.5}$$

Where, ψ defines the axisymmetric stream function which is expressed in terms of velocity components as $u=r^{-1}\psi_r$ and $v=-r^{-1}\psi_x$, $\theta(\eta)$ expresses dimensionless temperature and local the similarity variable is η.

Using Eq. (3.5), Eqs. (3.1-3.3) reduce into the following ODEs:

$$f'''+\frac{\left\{2(1+\Lambda)^{\frac{n-1}{2}}+(n-1)\Lambda(1+\Lambda)^{\frac{n-3}{2}}\right\}Mf''+ff''-Ha^2(f'-A)+\gamma\theta-f'^2+A^2}{\left((1+\Lambda)^{\frac{n-1}{2}}+(n-1)\Lambda(1+\Lambda)^{\frac{n-3}{2}}\right)(1+2M\eta)}=0, \tag{3.6}$$

$$\frac{1}{Pr}\{(1+2M\eta)\theta''+2M\theta'\}+f\theta'-f'\theta=0, \tag{3.7}$$

Corresponding boundary conditions are transformed as follows:

$$\begin{aligned} f(0) = 0,\ \ f'(0) = \ 1,\ \ \theta(0) = 1, \\ f'(\eta) \to A,\ \ \theta(\eta) \to 0 \quad \text{as } \eta \to \infty. \end{aligned} \tag{3.8}$$

In Eqs. (3.8)-(3.10), $M = (\nu L/u_0 R^2)^{1/2}$ is termed as curvature parameter, $K = (\lambda u_0/L)Re_x^{1/2}$ defines local Weissenberg number in which $Re_x = u_0 x^2/L\nu$ gives local Reynolds number and $\Lambda = (1 + 2M\eta)K^2 f''^2$, $Ha = \left(\sigma {B_0}^2 L/\rho u_0\right)^{1/2}$ shows magnetic interaction parameter, Prandtl number is expressed as $Pr = \ \eta_0 c_p/k$, velocity ratio parameter is denoted by $A = u_1/u_0$ and $\gamma = g\beta bL/u_0^2$ is the mixed convection parameter representing the strength of buoyant force.

The buoyant force expression will be positive and negative in the upper half ($x > 0$) and lower half where $x < 0$ respectively, When $\gamma > 0$ (b is positive). In this case, the buoyant force applies in the same direction in which the flow occurs and thus supports the fluid movement.

On the other hand, in the upper and lower halves when $\gamma < 0$ buoyant force becomes negative and thus it opposes the fluid movement.

Let us denote the local skin friction coefficient by C_f. It has prime importance in numerous applications. It can be defined via following formulae:

$$C_f = \frac{\tau_w}{\rho u_w^2/2}, \tag{3.9}$$

where τ_w stands for shear stress at the cylinder surface which can be evaluated as follows:

$$\tau_w = \tau_{xr}|_{r=R} = \eta_0 \left[\left(\frac{\partial u}{\partial r}\right) \left\{ 1 + \left(\lambda \left(\frac{\partial u}{\partial r}\right) \right)^2 \right\}^{\frac{n-1}{2}} \right]_{r=R}. \tag{3.10}$$

Using Eq. (3.10), Eq. (3.9) can be shown as:

$$\frac{1}{2}\, Re_x^{1/2}\, C_f = f''(0)\{1 + (Kf''(0))^2\}^{\frac{n-1}{2}}, \tag{3.11}$$

Another main quantity is the Nusselt number which is denoted as Nu_x. It can be evaluated from the following expression:

$$Nu_x = -\frac{x(\partial T/\partial r)_{r=R}}{(T_w - T_\infty)} = -Re_x^{1/2}\theta'(0). \tag{3.12}$$

3.3 Particular cases

3.3.1 Flat surface case

Stagnation-point flow of Carreau fluid flow striking on a vertical flat surface is attained when $M = 0$ or $R \to \infty$. In this case, the governing equations take the forms:

$$f''' + \frac{ff'' - Ha^2(f' - A) - f'^2 + \gamma\theta + A^2}{(1 + K^2 f''^2)^{\frac{n-1}{2}} + (n-1)(K^2 f''^2)(1 + K^2 f''^2)^{\frac{n-3}{2}}} = 0, \tag{3.13}$$

$$\frac{1}{Pr}\theta'' + f\theta' - f'\theta = 0, \tag{3.14}$$

with the same boundary conditions (3.8).

3.3.2 Newtonian fluid case

When $K = 0$, the governing system collapses to the Newtonian fluid case. In this situation, the relevant equations are given below:

$$(1 + 2M\eta)f''' + 2Mf'' + ff'' - Ha^2(f' - A) + \gamma\theta - f'^2 + A^2 = 0, \tag{3.15}$$

$$\frac{1}{Pr}\{(1 + 2M\eta)\theta'' + 2M\theta'\} + f\theta' - f'\theta = 0, \tag{3.16}$$

subject to the same boundary conditions (3.8).

3.4 Method of solution

The two-point boundary value problem represented by Eqs. (3.6-3.8) is figured out numerically first by using shooting technique via 5th order Runge-Kutta integration approach and additionally MATLAB built-in function bvp4c is also applied to attest the solutions. However, before utilizing the Runge–Kutta integration approach, the governing differential equations are reduced into a set of first order ODEs by making following substitutions:

$$\begin{pmatrix} Y_1 \\ Y_2 \\ Y_3 \\ Y_4 \\ Y_5 \end{pmatrix} = \begin{pmatrix} f \\ f' \\ f'' \\ \theta \\ \theta' \end{pmatrix}, \tag{3.17}$$

The corresponding system is:

$$\begin{pmatrix} Y_1 \\ Y_2 \\ Y_3 \\ Y_4 \\ Y_5 \end{pmatrix}' = \begin{pmatrix} Y_2 \\ Y_3 \\ -\dfrac{\left\{2(1+\Lambda)^{\frac{n-1}{2}} + (n-1)\Lambda(1+\Lambda)^{\frac{n-3}{2}}\right\} MY_3 - Ha^2(Y_2 - A) - Y_2^2 + Y_1Y_3 + \gamma\theta + A^2}{\left\{(1+\Lambda)^{\frac{n-1}{2}} + (n-1)\Lambda(1+\Lambda)^{\frac{n-3}{2}}\right\}(1+2M\eta)} \\ Y_5 \\ -\dfrac{[2MY_5 + Pr\{Y_1Y_5 - Y_2Y_4\}]}{(1+2M\eta)} \end{pmatrix}, \tag{3.18}$$

and requisite initial conditions are

$$\begin{pmatrix} Y_1 \\ Y_2 \\ Y_3 \\ Y_4 \\ Y_5 \end{pmatrix}_{\eta=0} = \begin{pmatrix} 0 \\ 1 \\ g_1 \\ 1 \\ g_2 \end{pmatrix}, \tag{3.19}$$

To integrate the system (3.18), we require suitable values of the unknown initial conditions $f''(0) = g_1$ and $\theta'(0) = g_2$. In shooting method unknown initial guess values g_1 and g_2 are estimated through Newton Raphson method until the boundary conditions at infinity $f'(\eta) \to A,\ \theta(\eta) \to 0$ as $\eta \to \infty$ are satisfied. Different values of η (such as η = 5, 10, 20 etc.) are taken in our numerical computations so that results are independent of η chosen.

3.5 Results and discussion

The numerical scheme described above is utilized to obtain graphical results of velocity and temperature fields for different choices of embedded parameters. We begin with analyzing how boundary layers adjacent to the stretching cylinder are affected by the presence of buoyant force. In this connection, profiles of f', proportional to u-velocity component, are derived by changing the values of mixed convection parameter γ. As expected, axial flow generated by the stretching effect of the cylinder is assisted by the presence of buoyant force. This result remains valid irrespective of the choice of velocity ratio parameter A. Following observations are is also noted from the graphs of Fig. 3.1. When free stream velocity is lower than the cylinder velocity, boundary

layer becomes increasingly thicker for increasing strength of buoyant force. However, such outcome is reversed when free stream velocity is higher than the velocity of stretching cylinder. The contribution of buoyant force term on the thermal boundary layer formation can be described from Fig. 3.2. Radial flow at the far field accelerates because of increasing buoyant force strength. This effect increases relative importance of the heat convection term, and thus reduces thermal boundary layer thickness.

Graphical representations of axial velocity profiles for varying Lorentz force strength are presented in the Fig. 3.3. The presence of transverse magnetic field opposes momentum transport by the cylindrical surface and hence thins the momentum boundary layer. It takes lower value of η for the velocity profile to approach its ambient value when higher magnetic field strength is applied. Results of Fig. 3.4 suggest that the heat convection term weakens with increasing Ha, due to a reduced entrained flow. As a result, heat conduction effect is accordingly amplified. Such tendency can be depicted from the graphs of θ computed at different values of Ha in Fig. 3.4.

Next, we discuss the contribution of curvature parameter on the boundary layer formed near a stretchable cylinder. It should be noticed that parameter M is proportional to the kinematic viscosity and thus one expects a progression in stream wise momentum diffusion as curvature parameter M rises. Such observation can be witnessed through Fig. 3.5. Heat conduction term, represented by $(1 + 2M\eta)\theta'' + 2M\theta'$, is proportional to parameter M. Therefore, heat conduction effect is predicted to dominate convection effect whenever curvature effects are present. Hence, thermal boundary layer is seen to thicken upon increasing parameter M (see Fig.3. 6).

Shear-thinning behavior of the fluid on the resulting boundary layer can be studied through the plots of axial velocity profile computed at different values of flow behavior index n in Fig. 3.7. Since apparent viscosity η has a direct relationship with n when n lies in the range $0 \leq n \leq 1$. Therefore, an enhancement in n, is anticipated to support the stream wise momentum diffusion or boundary layer development, as witnessed from Fig. 3.7. For same reason, the axial flow is seen to accelerate when $A < 1$, while such outcome is reversed for $A > 1$.

Fig. 3.8 illustrates the behavior of velocity f' for different values of Weissenberg number K. For $A < 1$, velocity decreases whenever K becomes large whereas, this result is reversed when $A > 1$. An enhancement in parameter K can be regarded as a growth in fluid relaxation time.

For a higher relaxation time, the boundary layer does not increase as quickly as it would for a fluid with a smaller relaxation time.

In order to see how shear stress exerted at the wall is affected by the shear-thinning character of the fluid, plots of skin friction coefficient with flow behavior index n are computed at different curvature parameters (see Fig. 3.9). It is predicted that lesser driving force will be needed at the cylindrical surface whenever larger n is accounted. Furthermore, Fig. 3.10 shows that heat transfer rate slightly rises whenever shear-thinning effect is strengthened.

Tables 3.1 and 3.2 compare the numerical data of $f''(0)$ and $\theta'(0)$ obtained by both shooting method and bvp4c. Numerical results are exactly same using both numerical schemes. It is concluded that shear stress exerted at the surface is proportional to the Weissenberg number K. Moreover, the effect of magnetic field is such that force required to stretch the cylindrical surface is increased in the existence of magnetic field. On the other hand, heat transfer rate from the solid surface is proportionate with the magnetic interaction parameter as evident from last column of this table 3.1 or table 3.2.

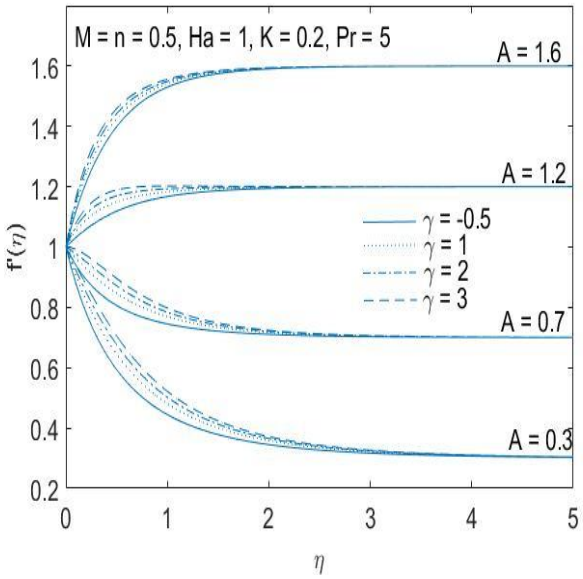

Fig. 3.1: Distribution of axial velocity field for varying choices of mixed convection parameter γ.

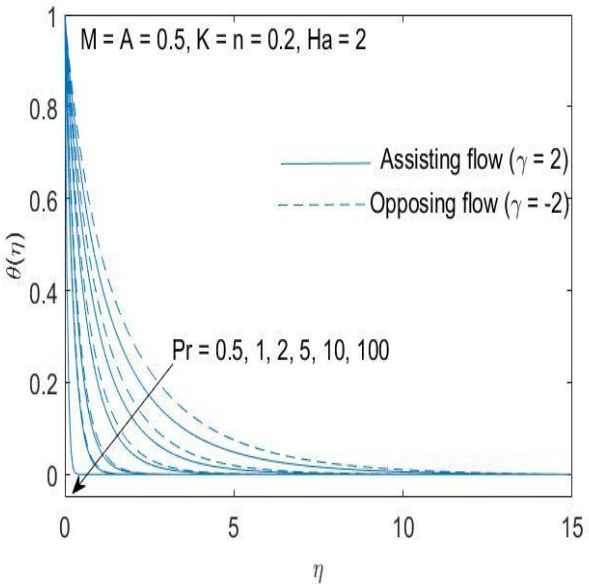

Fig. 3.2: Distribution of temperature field for a variety of Pr value.

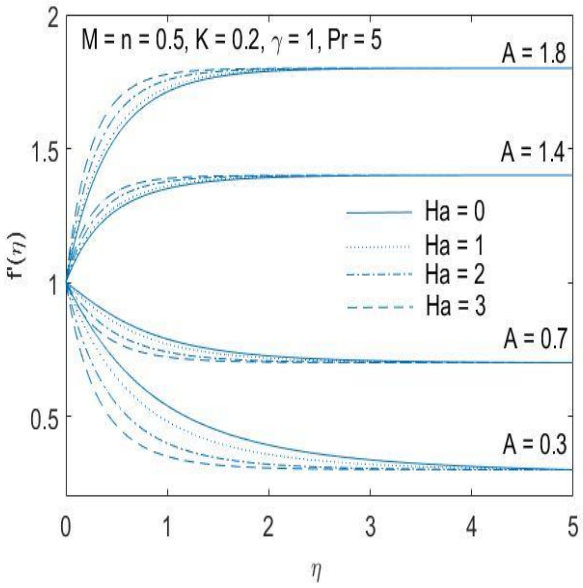

Fig. 3.3: Distribution of axial velocity field for various values of magnetic interaction parameter Ha.

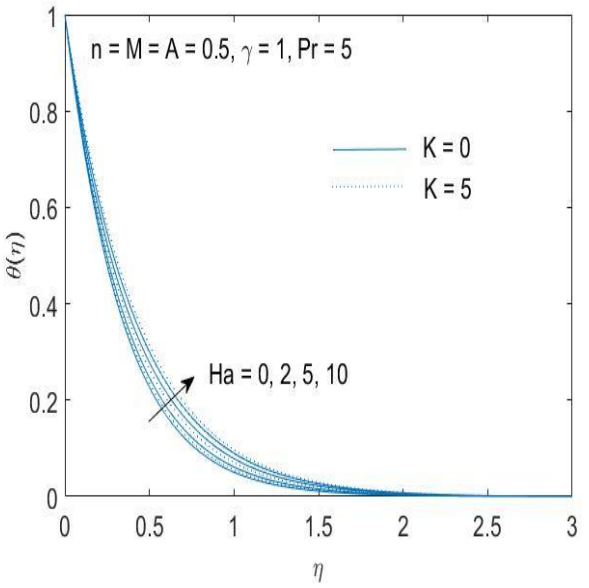

Fig. 3.4: Distribution of temperature field for various values of Ha values when $K = 0\ and\ K = 5$.

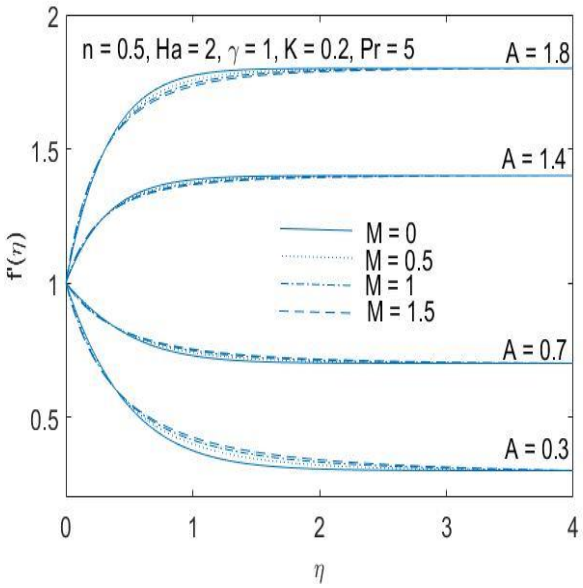

Fig. 3.5: Distribution of axial velocity field for various choices of curvature parameter M.

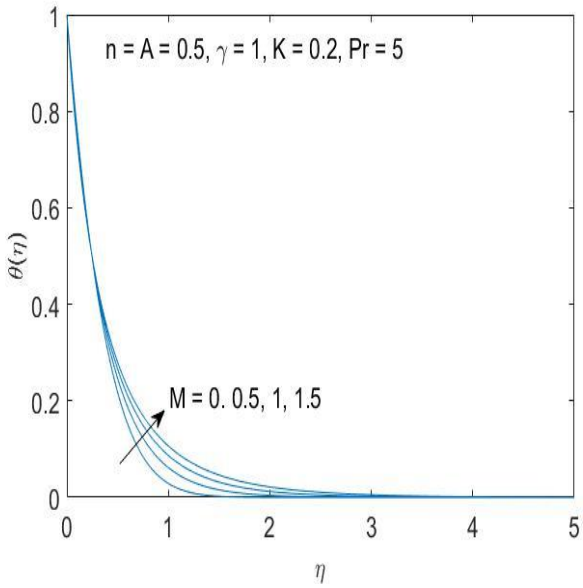

Fig. 3.6: Distribution of temperature field for a variety of M values.

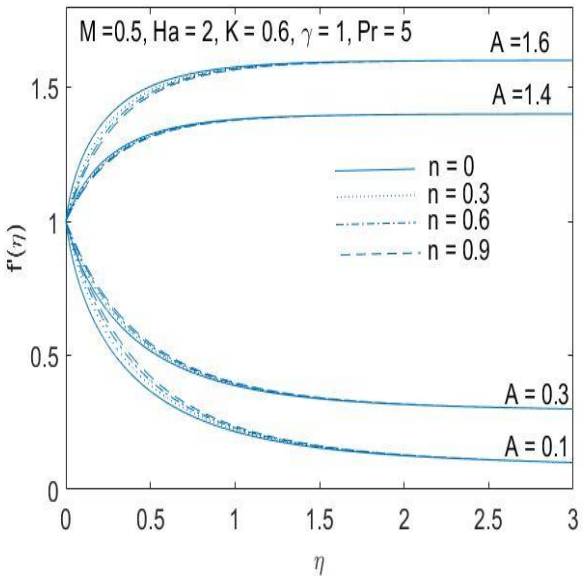

Fig. 3.7: Distribution of axial velocity field for various choices of flow behavior index n.

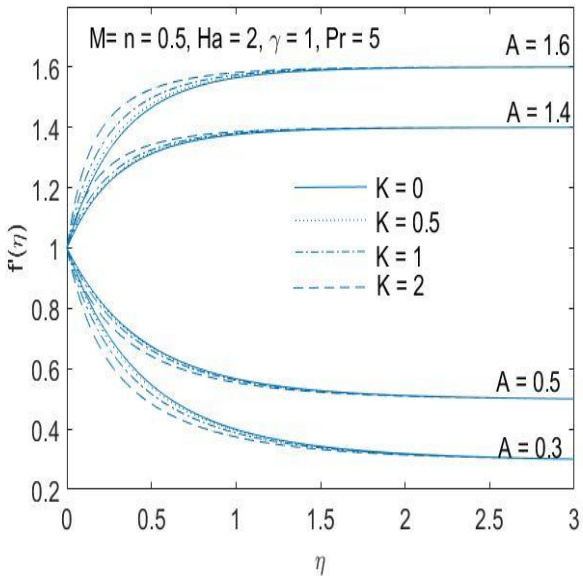

Fig. 3.8: Distribution of axial velocity field for various choices of local Wessienberg number K.

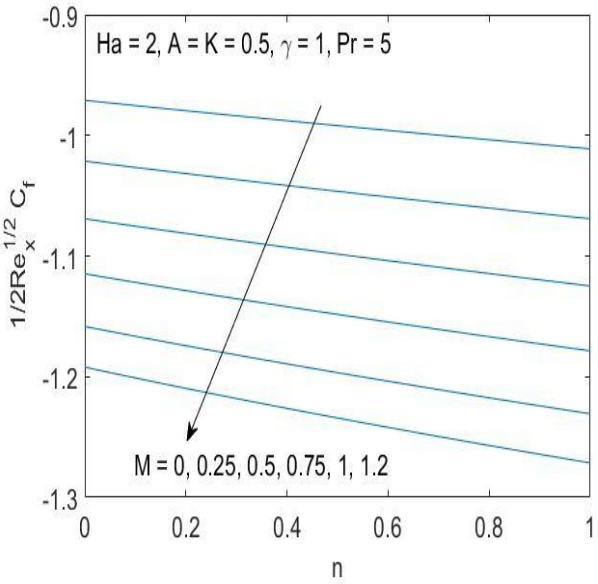

Fig. 3.9: Variation in skin friction coefficient with n for several values of curvature parameter M.

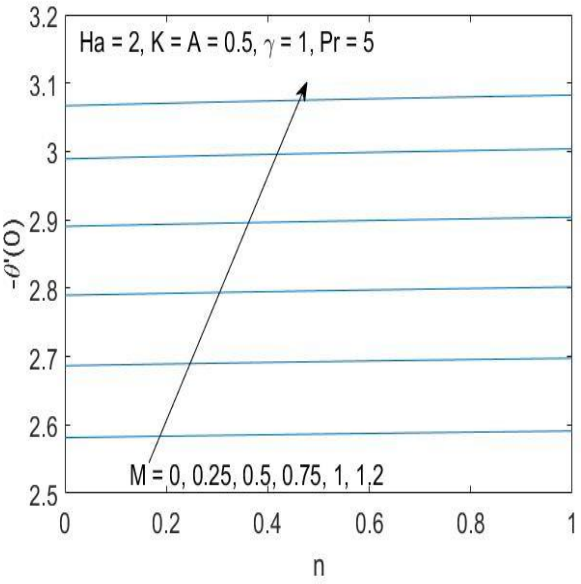

Fig. 3.10: Variation in Nusselt number with n for several values of curvature parameter M.

Table 3.1: Comparison of bvp4c and shooting method for special case of Flat Plate $M = 0, Pr = 5, n = 0.5$.

K	A	Ha	$\gamma = -1$		$\gamma = 1$	
			$f''(0)$	$\theta'(0)$	$f''(0)$	$\theta'(0)$
0	0.3	0	-1.0860 (-1.0860)	-2.5674 (-2.5674)	-0.6216 (-0.6216)	-2.6405 (-2.6405)
		0.5	-1.1518 (-1.1518)	-2.5532 (-2.5532)	-0.6922 (-0.6922)	-2.6262 (-2.6262)
	1.5		0.7568 (0.7568)	-2.9470 (-2.9470)	1.1266 (1.1266)	-2.9822 (-2.9822)
0.5	0.3		-1.3272 (-1.3272)	-2.5324 (-2.5324)	-0.7145 (-0.7145)	-2.6212 (-2.6212)
1			-2.7493 (-2.7493)	-2.4379 (-2.4379)	-0.7870 (-0.7870)	-2.6061 (-2.6061)
2			-31.4587 (-31.4587)	-1.9378 (-1.9378)	-1.1359 (-1.1359)	-2.5482 (-2.5482)

Table 3.2: Comparison of bvp4c and shooting method for Newtonian Case $n = 0.5, Pr = 5$ and $K = 0$.

M	A	Ha	$\gamma = -1$		$\gamma = 1$	
			$f''(0)$	$\theta'(0)$	$f''(0)$	$\theta'(0)$
1	0.3	0	-1.3876 (-1.3876)	-2.9552 (-2.9552)	-0.8812 (-0.8812)	-3.0366 (-3.0366)
	1.5		0.9473 (0.9473)	-3.4220 (-3.4220)	1.3277 (1.3277)	-3.4557 (-3.4557)
	0.3	0.5	-1.4586 (-1.4586)	-2.9398 (-2.9398)	-0.9592 (-0.9592)	-3.0207 (-3.0207)
	1.5		0.9836 (0.9836)	-3.4260 (-3.4260)	1.3591 (1.3591)	-3.4589 (-3.4589)
0.5	0.3	0.5	-2.7493 (-2.7493)	-2.4379 (-2.4379)	-0.7870 (-0.7870)	-2.6061 (-2.6061)
2			-31.4587 (-31.4587)	-1.9378 (-1.9378)	-1.1359 (-1.1359)	-2.5482 (-2.5482)

3.6 Concluding remarks

Stagnation-point of Carreau fluid impinging on a vertical heated cylindrical surface is formulated. Numerical simulations are made to investigate the contributions of buoyant force shear-thinning character of the fluid. Major observations of the study are listed below:

An enhancement of curvature effects increases the stream wise momentum diffusion which leads to a thicker momentum boundary layer.

Resisting force on the cylindrical surface is seen to grow considerably as curvature effects are increased. Curvature effects also amplify the heat transfer rate from the cylindrical boundary.

As per expectation, axial flow is considerably accelerated whenever shear-thinning effects are strengthened. Force required to stretch the cylinder increases as values of n are incremented.

Buoyant force acts as favorable/adverse pressure gradient for positive/negative values of the curvature parameter.

Shear stress at the cylindrical surface is declined while heat transfer rate is enhanced whenever buoyant force is present.

Present flow model simplifies when $M = 0$ or $R \to \infty$ (flat surface case). Moreover, the problem collapses to the Newtonian fluid situation when $K = 0$.

Bibliography

1. W. Ostwald, Ueber die rechnerische Darstellung des Strukturgebietes der Viskosität, Kolloid-Zeitschrift 47 (1929) 176–187.
2. M. M. Cross, Rheology of non-Newtonian fluids: A new flow equation for pseudoplastic systems, J. Colloid Sci. 20 (1965) 417–437.
3. P. J. Carreau, Rheological equations from molecular network theories, Trans. Soc. Rheol. 16 (1972) 99–127.
4. N. Ali and T. Hayat, Peristaltic motion of a Carreau fluid in an asymmetric channel, Appl. Math. & Comput. 193 (2007) 535-552.
5. T. Hayat, N. Saleem and N. Ali, Peristaltic flow of a Carreau fluid in a channel with different wave forms, Numer. Meth. Partial Diff. Eq. 26 (2010) 519-534.
6. N. S. Akbar and S. Nadeem, Carreau fluid model for blood flow through a tapered artery with a stenosis, Ain Shams Eng. J. 5 (2014) 1307-1316.
7. S. M. Kayani, S. Hina and M. Mustafa, A new model and analysis for peristalsis of Carreau–Yasuda (CY) nanofluid subject to wall properties, Arab. J. Sci. & Eng. 45 (2020) 5179-5190.
8. S. Hina, S. M. Kayani and M. Mustafa, Aiding or opposing electro-osmotic flow of Carreau–Yasuda nanofluid induced by peristaltic waves using Buongiorno model, Waves Rand. & Comp. Med. (2022); 10.1080/17455030.2021.2024299.
9. P. T. Griffiths, Flow of a generalised Newtonian fluid due to a rotating disk, J. Non-Newtonian Fluid Mech. 221 (2015) 9-17.
10. R. Malik, H. Sadaf and F. Dastar, Analysis of Carreau fluid flow by convectively heated disk with viscous dissipation effects, Zeitschrift für Naturforschung A 75 (2020) 825-832.
11. M. Khan, T. Salahuddin, R. Ali and Q. Khan, Heat transfer in generalized Carreau fluid flow near a radioactive heated rotating disk, Waves in Rand. & Comp. Med. (2021); DOI: 10.1080/17455030.2021.1979276.
12. I. L. Animasaun and I. Pop, Numerical exploration of a non-Newtonian Carreau fluid flow driven by catalytic surface reactions on an upper horizontal surface of a paraboloid of revolution, buoyancy and stretching at the free stream, Alexandria Eng. J. 56 (2017) 647-658.

13. M. Khan, H. Sardar, M. M. Gulzar and A. S. Alshomrani, On multiple solutions of non-Newtonian Carreau fluid flow over an inclined shrinking sheet, Res. Phys. 8 (2018) 926-932.
14. Y. Yun, S. Jee and J. Lee, Unsteady flow of Carreau fluids around an impulsively moving cylinder, Phys. Fluids 32 (2020), Article ID: 123105.
15. K. Naganthran, I. Hashim and R. Nazar, Non-uniqueness solutions for the thin Carreau film flow and heat transfer over an unsteady stretching sheet, Int. Commun. Heat & Mass Transf. 117 (2020), Article ID: 104776.
16. C. Y. Wang, Viscous swirling flow over a stretching cylinder, Phys. Fluids 31 (1988) 466-468.
17. C. Y. Wang and C. Ng, Slip flow due to a stretching cylinder, Int. J. Non-Linear Mech. 46 (2011) 1191-1194.
18. S. Mukhopadhyay, MHD boundary layer slip flow along a stretching cylinder, Ain Shams Eng. J. 4 (2013) 317-324.
19. J. A. Khan and M. Mustafa, A numerical analysis for non-linear radiation in MHD flow around a cylindrical surface with chemically reactive species, Res. Phys. 8 (2018) 963-970.
20. S. Mukhopadhyay and A. Ishak, Mixed convection flow along a stretching cylinder in a thermally stratified medium, J. Appl. Math. 2012 (2012), Article ID: 491695.
21. T. Fang, J. Zhang, Y. Zhong and H. Tao, Unsteady viscous flow over an expanding stretching cylinder, Chin. Phys. Lett. 28 (2011) Article ID: 124707.
22. W. M. K. A. W. Zaimi, A. Ishak and I. Pop, Unsteady viscous flow over a shrinking cylinder, J. King Saud Univ.-Sci. 25 (2013) 143-148.
23. Z. Abbas, S. Rasool and M. M. Rashidi, Heat transfer analysis due to an unsteady stretching/shrinking cylinder with partial slip condition and suction, 6 (2015) 939-945.
24. M. Khan, A. Ahmed, M. Irfan and J. Ahmed, Analysis of Cattaneo–Christov theory for unsteady flow of Maxwell fluid over stretching cylinder, J. Therm. Anal. & Calorimetry 144 (2021) 145-154.
25. A. S. Butt, A. Ali and A. Mehmood, Numerical investigation of magnetic field effects on entropy generation in viscous flow over a stretching cylinder embedded in a porous medium, Energy 99 (2016) 237-249.
26. M. Tamoor, M. Waqas, M. I. Khan, A. Alsaedi and T. Hayat, Magnetohydrodynamic flow

of Casson fluid over a stretching cylinder, Res. Phys. 7 (2017) 498-502.

27. A. Ali, D. N. K. Marwat and S. Asghar, Viscous flow over a stretching (shrinking) and porous cylinder of non-uniform radius, Adv. Mech. Eng. (2019); Article ID: https://doi.org/10.1177/1687814019879842.
28. A. Ishak, R. Nazar, and I. Pop, Magnetohydrodynamic (MHD) flow and heat transfer due to a stretching cylinder, Energy Convers. & Manag. 49 (2008) 3265-3269. https://doi.org/10.1016/j.enconman.2007.11.013
29. R. N. Kumar, R. J. P. Gowda, A. M. Abusorrah, Y. M. Mahrous, N. H. Abu-Hamdeh, A. Issakhov, M. Rahimi-Gorji, and B. C. Prasannakumara, Impact of magnetic dipole on ferromagnetic hybrid nanofluid flow over a stretching cylinder, Phys. Scr. 96 (2021) 045215. https://iopscience.iop.org/article/10.1088/1402-4896/abe324/meta
30. T. Salahuddin, A. Hussain, M. Y. Malik, M. Awais, and M. Khan, Carreau nanofluid impinging over a stretching cylinder with generalized slip effects: using finite difference scheme, Results Phys. 7 (2017) 3090-3099. https://doi.org/10.1016/j.rinp.2017.07.036
31. Hashim, M. Khan and A. S. Alshomrani, Characteristics of melting heat transfer during flow of Carreau fluid induced by a stretching cylinder, Eur. Phys. J. Plus 8 (2017); doi: 10.1140/epje/i2017-11495-6.
32. Khan, S. Ullah, M. Y. Malik and A. Hussain, Numerical analysis of MHD Carreau fluid flow over a stretching cylinder with homogenous-heterogeneous reactions, Res. Phys. 9 (2018) 1141-1147.
33. Z. Iqbal, M. Khan, A. Ahmed, M. Hussain, M. Y. Malik and S. Hussain, Thermal enhancement in the mixed convective flow of unsteady Carreau nanofluid with slip conditions: A numerical study, Adv. Mech. Eng. 13 (2021) 1-14.
34. K. Hiemenz, Die Grenzschicht an einem in den gleichformigen Flussigkeitsstrom eingetauchten geraden Kreiszylinder, Dinglers Polytech. J. 326 (1911) 321-324.
35. T. R. Mahapatra, S.K. Nandy and A.S. Gupta, Magneto hydrodynamic stagnation-point flow of a power-law fluid towards a stretching surface, Int. J. Non. Linear Mech.44 (2009) 124-129.
36. M. Mustafa, A. Mushtaq, T. Hayat and A. Alsaedi, Model to study non-linear radiation heat transfer in the stagnation-point flow of power-law fluid, Int. J. Numer. Method. H. 25 (2015) 1107-1119.

37. G. C. Layek, B. Mandal, K. Bhattacharyya and A. Banerjee, Lie symmetry analysis of boundary layer stagnation-point flow and heat transfer of non-Newtonian power-law fluids over a nonlinearly shrinking/stretching sheet with thermal radiation, International Journal of Nonlinear Sciences and Simulations. 19 (2018) 415-426.
38. S. Dholey, On the fluid dynamics of unsteady separated stagnation-point flow of a power-law fluid on the surface of a moving flat plate, Eur. J. Mech. - BFluids. 70 (2018) 102-114. https://doi.org/10.1016/j.euromechflu.2018.03.001.
39. B. Xie and Y. M. Wang, Stagnation-point flow and heat transfer of power-law MHD fluid over a stretching surface with convective heat transfer boundary condition, Int. J. Numer. Method. H. 32 (2022) 265-282. https://doi.org/10.1108/HFF-12-2020-0770.
40. M. Khan, Hashim and A. S. Alshomrani, MHD stagnation-point flow of a Carreau fluid and heat transfer in the presence of convective boundary conditions, PLoS One. (2016) 1-22. https://doi.org/10.1371/journal.pone.0157180.
41. N. M. Arifin, S. N. Yusof and N. S. Ismail, Slip effects on MHD stagnation-point flow of Carreau fluid past a permeable shrinking sheet, Matter: Int. J. Sci. Technol. 3 (2017) 525-532. https://doi.org/10.20319/mijst.2017.32.525532
42. M. Khan, A. M. E. Shafey, T. Salahuddin and F. Khan, Chemically Homman stagnation-point flow of Carreau fluid, Phys. A: Stat. Mech. Appl. 551 (2021) 124066.